Supplementary material

Facile fabrication of three-dimensional NiCo$_2$O$_4$ hierarchical nanosheet-wire structure for high-performance supercapacitors

Junyan Huang[a], Jinjie Zhou[a], Lijun Liu[b], Yaxi Zheng[b], Yin Wang[b], Xing Chen*[b]

[a]Department of Safety Supervision and Management, Chongqing Vocational Institute of safety & Technology, Chongqing 404020, China

[b]School of Environmental and Chemical Engineering, Chongqing Three Gorges University, Chongqing 404100, China

*Corresponding author. Tel: +86 23 58102262; Fax: +86 23 58102262

E-mail address: cxyjxyc@126.com (X. Chen).

Electrochemical measurements

The cyclic voltammetry (CV), galvanostatic charging/discharging curves (GCD), and electrochemical impedance spectroscopy (EIS) measurements were performed on a CHI660E electrochemical workstation. In a standard three-electrode setup, the NiCo$_2$O$_4$ HNSW electrode (1 × 1 cm^2), Hg/HgO electrode, Pt electrode (1 × 1 cm^2), and 6 M KOH aqueous were employed as working electrode, reference electrode, counter electrode, and electrolyte, respectively. The frequency range of EIS measurement was 0.01~1.0×10^5 Hz with an amplitude of 5 mV. The asymmetric supercapacitor was assembled by using NiCo$_2$O$_4$ HNSW as the positive electrode and activated carbon (AC) as the negative electrode. The NKK membrane was used as the separator and the 6 M KOH solution was used as the electrolyte. The cycling stability was measured in a Land CT3001A battery tester.

The equations for the specific capacitance, energy density, power density, and mass ratio

The specific capacity (C_s, C g^{-1}) of the electrode were calculated according to equation S1 to S2. The specific capacitance (C_d, F g^{-1}), Energy density (E, Wh kg^{-1}), and Power density (P, W kg^{-1}) of the assembled asymmetric supercapacitor were calculated according to equation S3 to S5 [1, 2].
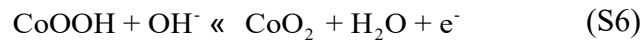
$$C_s = \frac{2I \int V dt}{m \Delta V} \qquad (S1)$$

$$C_d = \frac{I \Delta t}{m_d \Delta V} \qquad (S2)$$

$$E = \frac{1}{2 \times 3.6} C(\Delta V)^2 \qquad \text{(S3)}$$

$$P = \frac{3600E}{\Delta t} \qquad \text{(S4)}$$

When m (mg), m_d (mg), v (mV s^{-1}), I (A), and ΔV (V) represent the mass of the electrode, mass of electroactive materials in the assembled supercapacitor, scan rate, current density, and potential window, respectively. $\int Vdt$ and Δt (s) are the integrated area of the discharge curve and discharge time.

The probable redox peaks of the chemical transformations of Ni^{2+}/Ni^{3+} and Co^{2+}/Co^{3+}/Co^{4+}.

$$NiCo_2O_4 + OH^- + H_2O \ll NiOOH + 2CoOOH + e^- \qquad \text{(S5)}$$

$$CoOOH + OH^- \ll CoO_2 + H_2O + e^- \qquad \text{(S6)}$$

Charge storage mechanism and the calculation of the capacity contributions

Calculation of the parameter b [3].

$$i = av^b \qquad \text{(S7)}$$

Where v (mV s^{-1}) and i (A) is the scan rate and current density.

Calculation of the capacitive-controlled and diffusion-controlled contributions [4]:

$$i(V) = k_1v + k_2v^{1/2} \qquad \text{(S8)}$$

Where k_1v and $k_2v^{1/2}$ represent the values of the capacitive-controlled and diffusion-controlled processes.

Charge balance calculation

The mass ratio of the positive electrode and negative electrode was calculated based on the charge-balance equation.

$$\frac{m_+}{m_-} = \frac{C_- \Delta V_-}{C_+ \Delta V_+} \qquad \text{(S9)}$$

In equation S6, m_+ and m_- represent the mass of the positive and negative electrodes, respectively. C_+ and C_- are the capacitances. ΔV_+ and ΔV_- represent the potential windows, respectively.
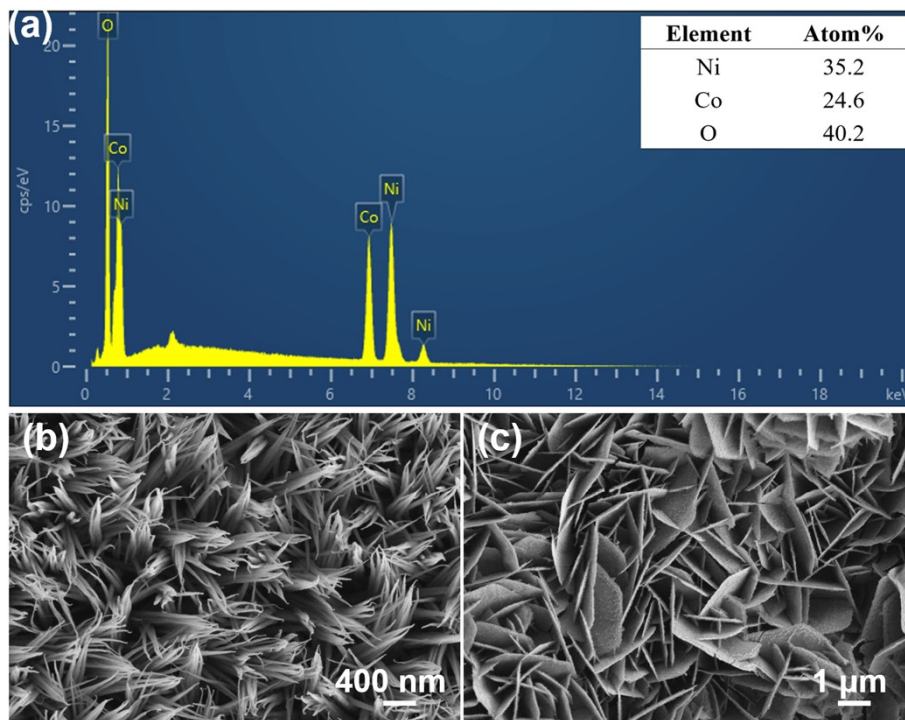
Fig. S1. (a) EDS elemental analysis. The SEM images of (b) $NiCo_2O_4$ NWs and (c) $NiCo_2O_4$ NSs
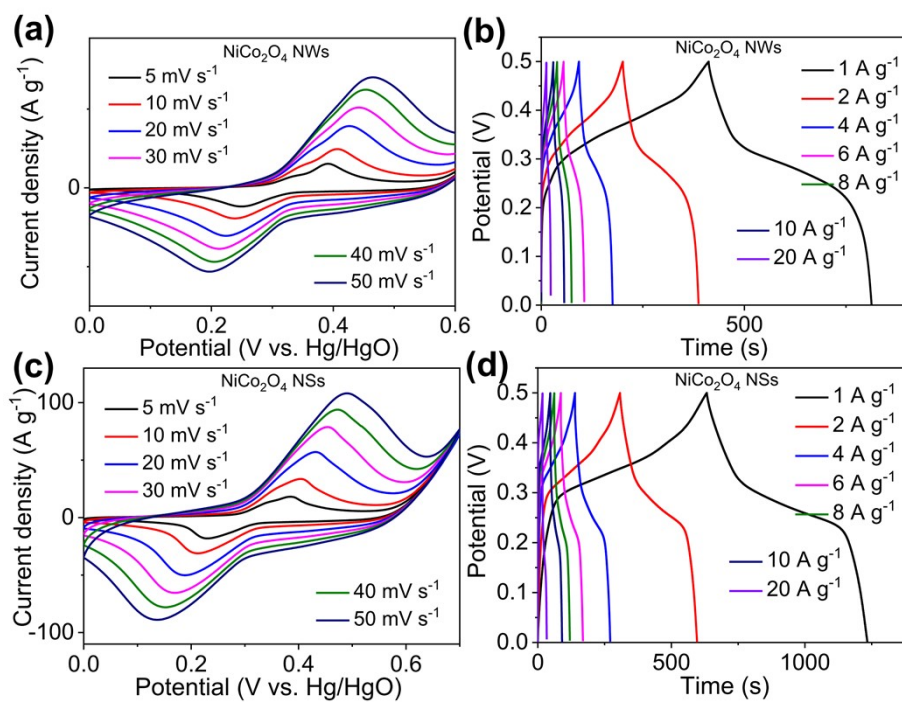

Fig. S2. CV and GCD curves of the (a, b) $NiCo_2O_4$ NWs and (c, d) $NiCo_2O_4$ NSs at different scan rates and current densities.
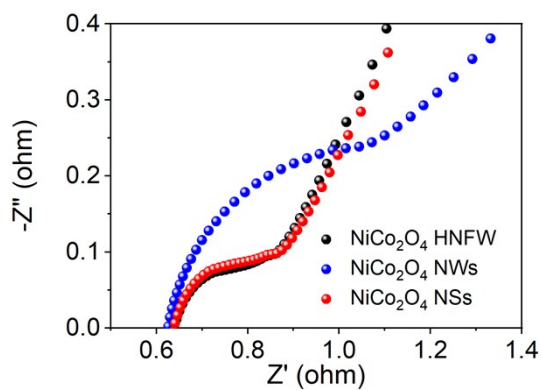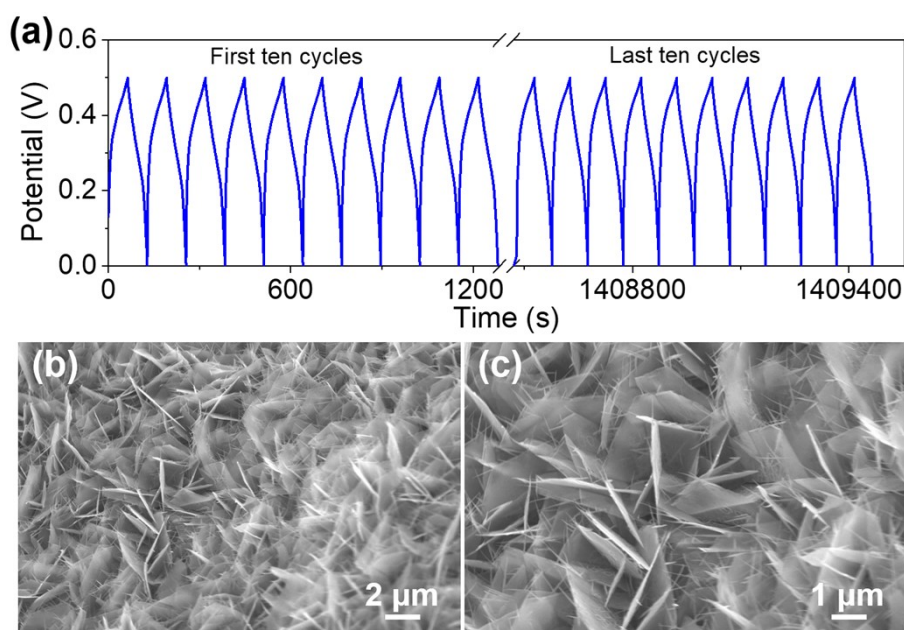
Fig. S3. The enlarged Nyquist plot.

Fig. S4. (a) GCD curves of the first ten cycles and the last ten cycles. (b, c) SEM images of the NiCo$_2$O$_4$ HNSW electrode after 12,000 charge-discharge cycles.

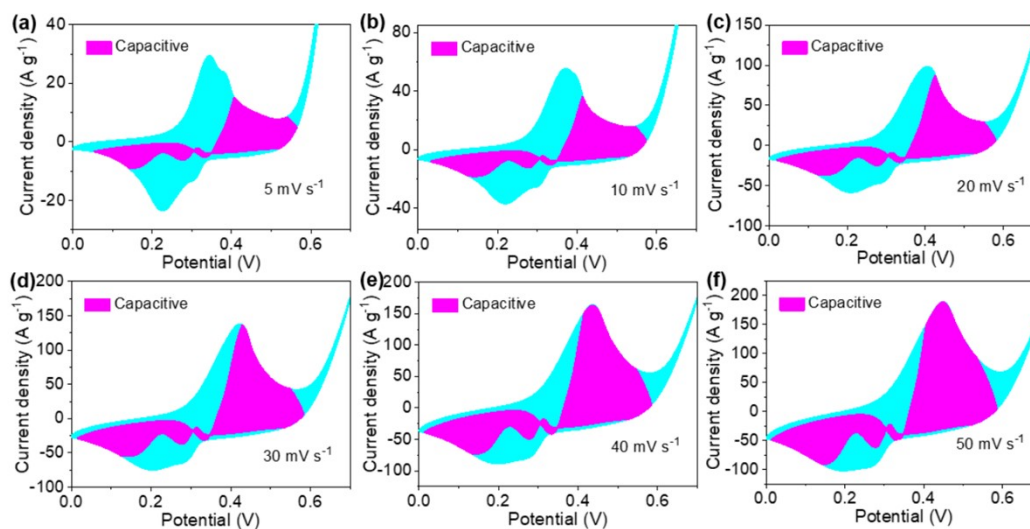Fig. S5. CV curves of the capacitive and diffusion-controlled processes of the NiCo$_2$O$_4$ HNSW

electrode at (a) 5, (b) 10, (c) 20, (d)30, (e) 40, and (f) 50 mV s^{-1}.
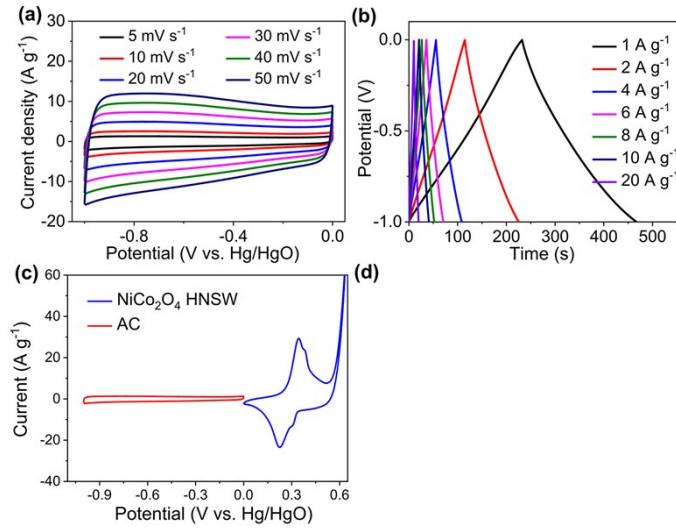

Fig. S6. (a, b) The CV and GCD curves of AC at different scan rates and current densities. (c) CV curves for NiCo$_2$O$_4$ HNSW and AC electrodes.

Table S1. The specific capacities (C g^{-1}) of NiCo$_2$O$_4$ HNSW, NiCo$_2$O$_4$ NWs, and NiCo$_2$O$_4$ NSs.

Material	1 A g^{-1}	2 A g^{-1}	4 A g^{-1}	6 A g^{-1}	8 A g^{-1}	10 A g^{-1}	20 A g^{-1}
NiCo$_2$O$_4$ HNSW	992.8	964.8	918.4	873.6	841.6	812.0	696.0
NiCo$_2$O$_4$ NWs	451.8	416.2	365.7	335.3	310.3	289.6	220.1
NiCo$_2$O$_4$ NSs	664.9	636.0	534.3	482.1	434.2	391.4	210.4

Table S2. Fitted results of the EIS data for NiCo$_2$O$_4$ HNSW, NiCo$_2$O$_4$ NWs, and NiCo$_2$O$_4$ NSs samples

Material	R$_s$ (Ω)	CPE1-T (mF)	CPE1-P (F)	R$_{ct}$ (Ω)	W1-R (Ω)	W1-T (Ω)	W1-P (Ω)	CPE2-T (F)	CPE2-P (F)
NiCo$_2$O$_4$ HNSW	0.65	0.077	1.2	0.014	0.55	0.047	0.28	0.27	1.0
NiCo$_2$O$_4$ NWs	0.63	2.2	0.90	0.31	4.9	6.2	0.37	0.24	0.79
NiCo$_2$O$_4$ NSs	0.67	0.13	1.2	0.018	0.41	0.030	0.25	0.30	0.95

Table S3. Comparison of specific capacitances with reported $NiCo_2O_4$-based electrode materials.

Material	Electrolyte	Capacitance retention	Specific capacitance (F g^{-1}) at 1 A g^{-1}	Reference
$NiCo_2O_4$@$MnMoO_4$ core-shell flowers	3 M KOH	87.8% (1 A g^{-1}, 5000 cycles)	1118	5
$NiCo_2O_4$ Nano flowers	6 M KOH	-	1030	6
$NiCo_2O_4$ Nanosheet	6 M KOH	90.9% (10 A g^{-1}, 5000 cycles)	2018	7
$NiCo_2O_4$ hexagonal nanostructures	2 M KOH	98.0% (10 A g^{-1}, 2000 cycles)	1525	8
$NiCo_2O_4$@$NiWO_4$ Core-shell Nanowire Arrays	6 M KOH	87.6% (5 A g^{-1}, 6000 cycles)	1384	9
$NiCo_2O_4$ Nanosheets	2 M KOH	99.0 % (10 A g^{-1}, 3000 cycles)	1472	10
$NiCo_2O_4$ Nanobelt/Graphene	6 M KOH	98.6 % (10 A g^{-1}, 3000 cycles)	1073	11
Mesoporous $NiCo_2O_4$ nanorods	2 M KOH	84.3% (5 A g^{-1}, 5000 cycles)	790	12
NNCO-1	3 M KOH	97.0% (2 A g^{-1}, 2000 cycles)	503.5 C g^{-1}	13
2D leaf-like NiCo2O4@CNPs	6 M KOH	97.3 % (2 A g^{-1}, 2000 cycles)	1265	14
$NiCo_2O_4$ HNSW	6 M KOH	77.0 % (10 A g^{-1}, 12,000 cycles)	1986 (992.8 C g^{-1})	**This work**

Table S4. The energy densities, power densities, and specific capacitances of the HSC device at different current densities.

Material	1 A g^{-1}	2 A g^{-1}	4 A g^{-1}	6 A g^{-1}	8 A g^{-1}	10 A g^{-1}	20 A g^{-1}
Specific capacitance (F g^{-1})	124.6	109.1	93.4	83.4	76.9	71.8	50.1
Power density (W kg^{-1})	800	1600	3200	4800	6400	8000	16000
Energy density (Wh Kg^{-1})	44.3	38.8	33.2	29.7	27.3	25.5	17.8

References

1 D. K. Kim, N. D. Kim, S. K. Park, K. D. Seong, M. Hwang, N. H. You and Y. Z. Piao, *J. Power Sources*, 2018, **380,** 55-63.

2 B. Huang, W. Wang, T. Pu, J. Li, C. Zhao, L. Xie and L. Chen, *Chem. Eng. J.*, 2019, **375,** 121969.

3 S. Shahrokhian and L. Naderi, *J. Phys. Chem. C*, 2019, **123,** 21353-21366.

4 F. Hekmat, H. Hosseini, S. Shahrokhian and H. E. Unalan, *Energy Storage Mater.*, 2020, **25,** 621-635.

5 Z. X. Gu and X. J. Zhang, *J. Mater. Chem. A*, 2016, **4,** 8249-8254.

6 R. Packiaraj, P. Devendran, K. S. Venkatesh, K. Mahendraprabhu and N. Nallamuthu, *J. Energy Storage*, 2021, **34,** 102029.

7 X. Zhang, F. Yang, H. Chen, K. Wang, J. Chen, Y. Wang and S. Song, *Small*, 2020, **16,** 2004188.

8 J. Bhagwan, G. Nagaraju, B. Ramulu, S. C. Sekhar and J. S. Yu, *Electrochim. Acta*, 2019, **299,** 509-517.

9 S. Chen, G. Yang, Y. Jia and H. Zheng, *J. Mater. Chem. A*, 2017, **5,** 1028-1034.

10 J. Wu, P. Guo, R. Mi, X. Liu, H. Zhang, J. Mei, H. Liu, W.-M. Lau and L.-M. Liu, *J. Mater. Chem. A*, 2015, **3,** 15331-15338.

11 J. Xu, L. Li, P. Gao, L. Yu, Y. Chen, P. Yang, S. Gai and P. Yang, *Electrochim. Acta*, 2015, **166,** 206-214.

12 J. Acharya, T. H. Ko, M.-K. Seo, M.-S. Khil, H.-Y. Kim and B.-S. Kim, *J. Colloid. Interf. Sci.*, 2020, **564,** 65-76.

13 D. T. Phat, P. M. Thao, N. Van Nghia, L. T. Son, T. V. Thu, N. T. Lan, N. Q. Quyen, N. Van Ky and T. Van Nguyen, *J. Energy Storage*, 2021, **33,** 102030.

14 H. Guan, N. Wei, M. Yang, J. Cheng, W. He and B. Zhang, *Vacuum*, 2023, **209,** 111812.